

Chapter 7

Time-Domain Nonlinear Acoustic Wave Modelling of Soft-Tissue Media

Abstract

A time-domain numerical code based on the constitutive relations of nonlinear acoustics is presented. To model frequency power law attenuation, such as observed in biological media, multiple relaxation processes are included and relaxation parameters are fitted to both exact frequency power law attenuation and empirically measured attenuation data of a variety of tissues. A computational technique based on artificial relaxation is included to correct the non-negligible numerical dispersion of the numerical method and to improve stability when shock waves are present. This technique avoids the use of high order finite difference schemes, leading to fast calculations. The accuracy of the method is discussed by comparison with analytical and k-space numerical solutions, and also to focused beam experimental data.

7.1 Introduction

The propagation of acoustics waves trough tissue for biomedical applications is usually linked to nonlinear propagation (Carstensen et al., 1980). Nonlinear regime is commonly achieved in therapy techniques in which the waves interact with the tissue to achieve some ultrasound bio-effect. On the other hand, most tissues shows very large acoustic attenuation coefficients at interest frequencies (Duck, 1990). Therefore, for most ultrasound imaging techniques the acoustic amplitude necessary to achieve a good signal/noise ratio is high enough to generate weakly nonlinear effects, while, in some applications, nonlinear effects are used as the basis of imaging and therapy techniques.

Thus, accurate prediction of finite amplitude acoustic waves traveling through biological media are essential in developing new therapy and imaging techniques for medical ultrasound applications (Carstensen et al., 1980; Muir et al., 1980). Numerous experimental studies show that attenuation $\alpha(f)$ of biological media exhibits a power law dependence on frequency $\alpha(f) = \alpha_0 f^\gamma$ over the frequency range used in medical applications (Hill et al., 2004; Duck, 1990). Considering an initial monochromatic plane wave traveling through nonlinear media, two opposite effects govern the final wave amplitude: on one hand, higher harmonics appear and their amplitude grows as a consequence of nonlinear progressive wave steepening; and on the other hand, the damping for each harmonic is different, following the above power law. Therefore, differences in the frequency power law model can lead to huge differences in attenuation of higher harmonics, and hence the inclusion of frequency dependence attenuation is critical for correctly predict nonlinear propagation.

7.1.1 Models of frequency power law media attenuation

Classical thermo-viscous sound attenuation exhibit a squared frequency dependence, $\gamma = 2$ (Pierce, 1989), however the empirically fitted power law for soft tissues typically ranges between $\gamma = (0.6, 2)$ (Goss et al., 1979; Duck, 1990; Hill et al., 2004). For most tissues the attenuation shows a dependence that can be modeled by γ close to the unity, where the specific value varies from different tissues. Moreover, for some individual examples the local value of γ exhibit lower values at low ultrasound frequencies and tends to 2 in the high frequency limit (Hill et al., 2004). Despite the study of the physical mechanism besides this complex frequency dependence is out of the scope of this work, there exist numerous phenomenological approaches for including the observed losses in the acoustic equations (Wismer et al., 1995; Kellya et al., 2009). On the other hand, is common in literature to describe the losses in soft tissues as multiple-relaxation processes (Nachman et al., 1990; Hill et al., 2004), from continuous distribution of relaxation processes (Jongen et al., 1986) to a discrete representation. Thus, relaxation parameters can be

optimized to fit the observed tissue attenuation, where has been shown that two processes are enough to model tissue attenuation with acceptable accuracy over frequency range covering about 4 octaves (Yang et al., 2005). Moreover, fractional partial differential operators can describe frequency power law attenuation (Caputo, 1967) when inserted into a wave equation. These operators can be included into wave modeling equations by means of time-causal convolutions (Szabo, 1994; Chen et al., 2003), fractional spatial derivatives (Chen et al., 2004) and its causal correction (Treeby et al., 2010), and combined time-space fractional derivatives (Caputo, 1967; Wismer, 2006). The latter operators can be biological motivated and derived from tissue micro-structure using fractal ladders based on networks of springs and dashpots (Kellya et al., 2009). However, these fractional loss operators can be also derived from a continuum of relaxation process (Nasholm et al., 2011), that suggest that the two approaches can be equivalent under certain conditions (Treeby et al., 2012).

7.1.2 Burgers equation

The above lossy operators can be included in a variety of nonlinear acoustic wave propagation models and, while analytical solutions are not available for finite amplitude waves in frequency power law media even in simplest configurations, a wide range of numerical methods has been developed. The numerical resolution of the nonlinear constitutive equations in tissue-like medium supposes a difficult problem due to the large size of the region of interest in relation to the size of the acoustic wavelength and the complexity of the model. Simplifying assumptions have been needed in the past for modeling nonlinear propagation in the past. Forward or one-way methods are the simplest way to model progressive nonlinear acoustic waves. The general representation of a causal media response was introduced in the Burgers equation (Blackstock, 1985) leading to the generalized Burgers equation. Thus, by choosing an adequate time function in the convolution kernel the attenuation and dispersion of an specific medium can be accurately modeled. The memory function can be modeled by a discrete sum of relaxation processes (Cleveland et al., 1996), while fractional time derivatives can also be included into the augmented Burgers equation (Ochmann et al., 1993).

7.1.3 KZK and one-way models

In order to describe finite amplitude sound beam diffraction effects in a paraxial approximation the well-known Khokhlov-Zabolotskaya-Kuznetsov equation (KZK) (Aanonsen et al., 1984; Lee et al., 1995) can be used. The KZK model can be extended for accounting for tissue attenuation by including relaxation (Cleveland et al., 1996; Yang et al., 2005) or fractional derivatives (Prieur et al., 2011). The KZK equation is commonly solved by a split operator techniques (Lee et al., 1995) that allows the frequency domain representation of the progressive wave. In this

way, the inclusion of tissue attenuation can be achieved efficiently in frequency domain (Khokhlova et al., 2006). Efficient and fast numerical solutions of the KZK model in power law media are also feasible under the assumption of Gaussian representation of the transverse field for each harmonic (Soneson et al., 2007). To overcome the validity of the parabolic approximation (i.e. when dealing with large aperture focused sound sources or modeling sound field near the acoustic source) many approaches has been proposed (Varslot et al., 2005). Also other phenomenological one-way approximations of finite amplitude sound beams has been developed (Christopher et al., 1991; Tavakkoli et al., 1998) and extended including tissue attenuation (Zemp et al., 2003). Furthermore, a numerical solution of the one-way version of the Westervelt equation (Yuldashev et al., 2011) has been also proposed.

7.1.4 Full-wave Westervelt type equations

Tissue inhomogeneity can be modeled in these one-way models (Jing et al., 2007), like transmission though tissue layers with refraction, but they do not take into account backscattering and multiple reflections. More realistic models, e.g. those accounting for scattering from internal tissue structures, are based on the Westervelt-type full-wave equations. Finite-Differences in Time-Domain methods (FDTD) can be applied to obtain explicit numerical schemes that account for nonlinear propagation and temperature rising in thermo-viscous media (Hallaj et al., 1999), where the inclusion of temperature-dependent sound speed changes can be also modeled (Hallaj et al., 2001). Tissue attenuation can be achieved in the Westervelt nonlinear wave equation by including multiple relaxation processes (Pinton et al., 2009) with optimized relaxation parameters. The Westervelt equation can be solved also by the Iterative Nonlinear Contrast Source (INCS) (Huijssen et al., 2010) where power law attenuation is modeled as a compliance relaxation function (Demi et al., 2011; Verweij et al., 2013). Other approach to include tissue losses in the Westervelt equation is to solve the model in k-space and directly include tissue looses in spatial frequency domain (Jing et al., 2012). This full-wave equation has been validated for strongly focused sources (Jing et al., 2011). However, due to the assumptions taken in the derivation of the Westervelt equation, the accuracy of this model is limited in practical situations as (*i*) the modeling of rigid boundaries where the thermo-viscous boundary layer effects are not-negligible, i.e. in general case where the particle velocity becomes rotational, (*ii*) situations where the second order Lagrangian density of acoustical energy not vanish, i.e. where plane progressive waves does not exist and the acoustic field becomes complex due to multiple scattering, reverberation or resonances, (*iii*) situations where the equilibrium-state particle velocity is not null, including the self generation of acoustic streaming. See Ref. Hamilton et al. (1998b) Chap. 3 for further discussion.

In this way, a physical model based on the constitutive relations of nonlinear

acoustics include a more complete description of the nonlinear acoustic phenomena over arbitrary boundary conditions, i.e. the time-space relations between the involved acoustic magnitudes remains exact.

7.1.5 Full-wave constitutive relations

The recent development of computational capacity has made possible to consider the full constitutive relations (i.e. without the assumptions discussed above). Thus, for small-amplitude acoustic waves, the linearized pressure-velocity formulation of constitutive relations in inhomogeneous media was solved by means of Finite-Differences in Time-Domain (FDTD) methods with frequency independent losses by Manry et al. (Manry et al., 1996), or using two-step MacCormack finite-differences scheme by Mast et al. (Mast et al., 1997). Also, relaxation processes can be included in finite difference methods in an efficient way in order to model tissue attenuation and dispersion (Yuan et al., 1999). Furthermore, k-space numerical methods have also been applied to solve the linearized first order equations in lossless inhomogeneous media (Mast et al., 2001). In order to account for soft tissue losses, the computational solution of the fractional Laplacian by k-space spectral methods have demonstrated to be extremely efficient due to the spatial frequency domain representation of the acoustic field (Treeby et al., 2010).

In the case of nonlinear constitutive relations models, the evolution of the acoustic magnitudes have been simulated in time-domain by means of finite differences schemes such as Dispersion Relation Preserving method (DRP) in ideal fluids and axisymmetric domains (Ginter et al., 2002). Thermo-viscous losses in finite-differences methods have been widely used, see Sparrow et al. (Sparrow et al., 1991). In order to introduce tissue attenuation in the governing equations time-dependent fractional derivatives can be included by convolutional operators. Thus, in Ref. Liebler et al. (2004) an efficient method has been presented, but although the memory requirements can be strongly reduced compared to direct convolutions the algorithm employs up to ten auxiliary fields and a memory buffer of three time steps. Furthermore, construction of specific causal memory functions that models soft tissue attenuation and dispersion in Navier-Stokes equations is also possible (Lobanova et al., 2014), but certain time history must be stored in memory and in this case the computational domain was restricted to one dimensional propagation.

In order to overcome those numerical limitations, recently k-space and pseudo-spectral numerical methods have been applied to constitutive relations in nonlinear regime to solve fractional Laplacian operators efficiently (Treeby et al., 2012). Furthermore, in the case of domains of hundreds of wavelengths, when the cumulative phase error due to numerical dispersion of standard finite-difference schemes can not be neglected, those spectral numerical methods have reported an improvement in accuracy of the numerical solution. This two factors, i.e. the negligible numerical dispersion and the efficient resolution of fractional Laplacian operators, have

led the spectral methods to be widely used in practical applications. However, their main limitation is that the implementation of natural space discontinuities due to tissue layers or rigid boundary conditions leads to errors in the reconstruction of the spectral information due to the poor convergence of Fourier series at jumps, i.e. the well-known Gibbs oscillations. Preventing this kind of errors is typically achieved by filtering the spatial spectrum (Jing et al., 2012), so the theoretical spatial minimum sampling of two point per wavelength becomes larger. In addition, these errors propagate globally and affect to the accuracy all over the domain, in contrast with locally propagating errors in finite differences methods. On the other hand, taking into account the spatial discontinuity due to symmetry boundary condition, axisymmetric domains becomes not feasible by standard k-space methods, and full 3D domains must be employed even for axisymmetric configurations. Those errors can be prevented by means of the recently developed Fourier Continuation (FC) method (Albin et al., 2012). However, the discontinuities formed due to shock propagation are still not solved by FC methods and other additional numerical treatment must be applied for correctly describe shock formation, e.g. intensive computations by high order accurate weighted essentially non-oscillatory schemes (FC/WENO) (Shahbazi et al., 2011). Unlikely, the computational times increases by using those intensive computational techniques and the multiresolution analysis to detect discontinuities in the domain.

The aim of the present chapter is to present a generalization of the constitutive relations of nonlinear acoustics including multiple relaxation processes in a non-convolutional formulation that allows the time-domain numerical solution by an explicit finite differences numerical scheme. Frequency power law attenuation based in relaxation have been applied in the same way than it has been applied to generalized Burgers equation (Cleveland et al., 1996), Khokhlov-Zabolotskaya-Kuznetsov (KZK) model (Cleveland et al., 1996; Yang et al., 2005) and Westervelt equation (Pinton et al., 2009). The relaxation parameters have been fitted to both exact frequency power law attenuation and empirically measured attenuation of a variety of tissues that does not fit an exact power law. Two processes have been enough to model tissue attenuation with acceptable accuracy over a frequency range covering about 4 octaves, as it was demonstrated by Yang et al. (Yang et al., 2005). A numerical technique based on artificial relaxation is included to control the non-negligible numerical dispersion of the FDTD method and improve stability when shock waves are present in the solution. The method includes backscattering and arbitrary propagation direction of finite amplitude beams, and can be specially suitable in axisymmetric configurations where the computational resources for full 3D k-space methods are prohibitive.

7.2 Generalized nonlinear acoustics model for multiple relaxation media

7.2.1 Full-wave modeling

The principles of mass and momentum conservation lead to the main constitutive relations for nonlinear acoustic waves, which for a fluid can be expressed as (Naugolnykh et al., 1998)

$$\frac{\partial \rho}{\partial t} = -\nabla \cdot (\rho \mathbf{v}) \tag{7.1}$$

and

$$\rho \left(\frac{\partial \mathbf{v}}{\partial t} + \mathbf{v} \cdot \nabla \mathbf{v} \right) = -\nabla p + \eta \nabla^2 \mathbf{v} + \left(\zeta + \frac{\eta}{3} \right) \nabla \left(\nabla \cdot \mathbf{v} \right), \tag{7.2}$$

where ρ is the total density field, $\mathbf{v}$ is the particle velocity vector, p is the pressure, and η and ζ are the coefficients of shear and the bulk viscosity respectively. The acoustic waves described by this model exhibit viscous losses with quadratic power law dependence on frequency. In order to include a power law frequency dependence on the attenuation, a multiple relaxation model will be added into the time domain equations.

The basic mechanism for energy loss in relaxing media is the appearance of a phase shift between the pressure and density fields. This behavior is commonly modeled as a time dependent relation at the fluid state equation, that for a fluid retaining the material nonlinear effects up to second order an be expressed as (Naugolnykh et al., 1998; Rudenko et al., 1977):

$$p = c_0^2 \rho' + \frac{c_0^2}{\rho_0} \frac{B}{2A} \rho'^2 + \int_{-\infty}^{t} G(t - t') \frac{\partial \rho'}{\partial t} dt, \tag{7.3}$$

where $\rho' = \rho - \rho_0$ is the density perturbation over the stationary density ρ_0, B/A is the nonlinear parameter, c_0 is the small amplitude sound speed, and $G(t)$ is the kernel associated with the relaxation mechanism. The first two terms of the right hand side of Eq. (7.3) describe the instantaneous response of the medium, where the convolutional third term accounts for the "memory time" of the relaxing media. Thus, by choosing an adequate time function for the kernel $G(t)$ the model can present an attenuation and dispersion response that fits the experimental data of the heterogeneous media. However, the direct resolution of the constitutive relations (7.1-7.3) in this integral form is a complex numerical task due to the convolutional operator. Thus, instead of describe $G(t)$ with a specific time domain waveform, the response of the heterogeneous medium can be alternatively described by a sum of N relaxation processes with exponential time dependence

as:

$$\int_{-\infty}^{t} G(t-t')\frac{\partial \rho'}{\partial t}dt = \sum_{n=1}^{N} G_n * \frac{\partial \rho'}{\partial t}, \tag{7.4}$$

with the n-th order relaxation kernel expressed as

$$G_n(t) = \eta_n c_0^2 \, \mathrm{e}^{\frac{-t}{\tau_n}} H(t), \tag{7.5}$$

where $H(t)$ is the Heaviside piecewise function $H(t<0)=0$, $H(t>0)=1$, τ_n is the characteristic relaxation time and η_n the relaxation parameter for the n-th order process. This last dimensionless parameter controls the amount of attenuation and dispersion for each process as $\eta_n = (c_n^2 - c_0^2)/c_0^2$, where c_n is the sound speed in the high frequency limit associated to n-th order relaxation process, also known as the speed of sound in the "frozen" state (Pierce, 1989). In order to describe relaxation without the need of including a convolutional operator, we shall define a state variable S_n for each process as

$$S_n = \frac{1}{\tau_n} G_n * \rho'. \tag{7.6}$$

Thus, using the convolutional property $\frac{\partial}{\partial t}\left(G(t) * \rho'(t)\right) = \frac{\partial G(t)}{\partial t} * \rho'(t) = G(t) * \frac{\partial \rho'(t)}{\partial t}$, the time derivative of the relaxation state variable obeys the following relation for the n-th order process:

$$\frac{\partial S_n}{\partial t} = \left(-\frac{1}{\tau_n}\frac{\eta_n c_0^2}{\tau_n} \mathrm{e}^{-\frac{t}{\tau_n}} H(t) + \frac{\eta_n c_0^2}{\tau_n} \mathrm{e}^{-\frac{t}{\tau_n}} \delta(t) \right) * \rho' \tag{7.7}$$

where $\delta(t)$ is the Dirac delta function. Using the Eq. (7.6) this relation becomes a simple ordinary differential equation for each process as

$$\frac{\partial S_n}{\partial t} = -\frac{1}{\tau_n} S_n + \frac{\eta_n c_0^2}{\tau_n} \rho'. \tag{7.8}$$

Using again convolutional properties, we can substitute Eq. (7.8) into (7.4), and the relaxing nonlinear state Eq. (7.3) becomes

$$p = c_0^2 \rho' + \frac{c_0^2}{\rho_0}\frac{B}{2A}\rho'^2 - \sum_{n=1}^{N} S_n + \sum_{n=1}^{N} \eta_n c_0^2 \rho'. \tag{7.9}$$

Moreover, if "frozen" sound speed for N mechanisms is defined as $c_\infty^2 = c_0^2\left(1 + \sum_{n=1}^{N} \eta_n\right)$, Eq. (7.9) leads to

$$p = c_\infty^2 \rho' + \frac{c_0^2}{\rho_0}\frac{B}{2A}\rho'^2 - \sum_{n=1}^{N} S_n. \tag{7.10}$$

Due to the smallness of the relaxation parameter, η_n, i.e. when weak dispersion is modeled, the sound speed in the high frequency limit reduces to (Naugolnykh et al., 1998):

$$c_\infty = c_0 \left(1 + \sum_{n=1}^{N} \frac{\eta_n}{2} \right). \tag{7.11}$$

Note Eq. (7.10) for a mono-relaxing media is equivalent to that can be found in literature (Rudenko et al., 1977)

$$p = c_\infty^2 \rho' + \frac{c_0^2}{\rho_0} \frac{B}{2A} \rho'^2 - \int_{-\infty}^{t} \frac{\eta c_0^2}{\tau} \mathrm{e}^{-\left(\frac{t-t'}{\tau}\right)} \rho'(t'). \tag{7.12}$$

Thus, the constitutive relations to solve by means of the numerical method in the nonlinear regime are the continuity Eq. (7.1), the motion Eq. (7.2) and the second order fluid state relaxing Eq. (7.10), where the state variable S_n obeys the relation (7.8) for the n-th order relaxation process. Although the aim of this work is to model biological media, the generalized formulation presented here can be used to describe the attenuation and hence the dispersion observed in other relaxing media, as the relaxation processes of oxygen and nitrogen molecules in air or the relaxation associated with boric acid and magnesium sulfate in seawater (Pierce, 1989).

7.2.2 Small amplitude modeling

If small amplitude perturbations are considered, an equivalent derivation of this model can be expressed for multiple relaxation media (Yuan et al., 1999). Thus, for an homogeneous inviscid relaxing fluid the linearized continuity and motion Eq. (7.1-7.2) reduces to

$$\frac{\partial \rho}{\partial t} = -\rho_0 \nabla \cdot \mathbf{v} \tag{7.13}$$

and

$$\rho_0 \frac{\partial \mathbf{v}}{\partial t} = -\nabla p, \tag{7.14}$$

and linearizing the fluid state Eq. (7.10) we obtain:

$$\rho' = \frac{1}{c_\infty^2} \left(p + \sum_{n=1}^{N} S_n \right). \tag{7.15}$$

These equations can be solved directly in this form, however, if expressed in pressure-velocity formulation the density field is no longer necessary and computational effort can be reduced. Thereby, assuming a linear "instantaneous"

compressibility $\kappa_\infty = \rho_0 c_\infty^2$, and substituting Eq. (7.15) into Eq. (7.13) yields

$$\frac{\partial p}{\partial t} + \sum_{n=1}^{N} \frac{\partial S_n}{\partial t} = -\kappa_\infty \nabla \cdot \mathbf{v}. \tag{7.16}$$

Then, taking the time derivative of the state variable Eq. (7.8) we get

$$\frac{\partial p}{\partial t} - \sum_{n=1}^{N} \frac{1}{\tau_n} S_n + \rho' \sum_{n=1}^{N} \frac{\eta_n c_0^2}{\tau_n} = -\kappa_\infty \nabla \cdot \mathbf{v}. \tag{7.17}$$

Finally, substituting again the linearized state Eq. (7.15) and arranging terms the linearized continuity equation leads to

$$\frac{\partial p}{\partial t} + p \sum_{n=1}^{N} \frac{\eta_n c_0^2}{\tau_n c_\infty^2} + \sum_{n=1}^{N} \left(\frac{\eta_n c_0^2}{\tau_n c_\infty^2} - \frac{1}{\tau_n} \right) S_n = -\kappa_\infty \nabla \cdot \mathbf{v}. \tag{7.18}$$

On the other hand, the state evolution equation can be expressed as a function of the acoustic pressure as

$$\frac{\partial S_n}{\partial t} = -\frac{1}{\tau_n} S_n + \frac{\eta_n c_0^2}{\tau_n c_\infty^2} \left(p - \sum_{n=1}^{N} S_n \right). \tag{7.19}$$

Thus, the linearized governing Eq. (7.14, 7.18) for a relaxing media are expressed in a pressure-velocity formulation and can be solved together with the coupled state evolution equation (7.19) by means of standard finite differences numerical techniques (Yuan et al., 1999). In this way, lossless linear acoustics equations can be obtained by setting $\eta_n = 0$ or in the limit when the relaxation times $\tau_n \to \infty$. The relaxation behavior described by this linearized model is achieved too by the formulation described by (Yuan et al., 1999), where the relaxation coefficients η_n and the relaxation variable S_n are defined in a different, but analogous way.

7.3 Numerical solution by finite differences in time domain

In this section the numerical techniques for solving the complete set of equations (continuity Eq. (7.1), momentum Eq. (7.2), state Eq. (7.10) and the relaxation Eq. (7.8)) are presented. The numerical method is based on a second order FDTD method where multiple relaxation processes are included in order to: first, modeling physical attenuation and dispersion in the interest frequencies and second,

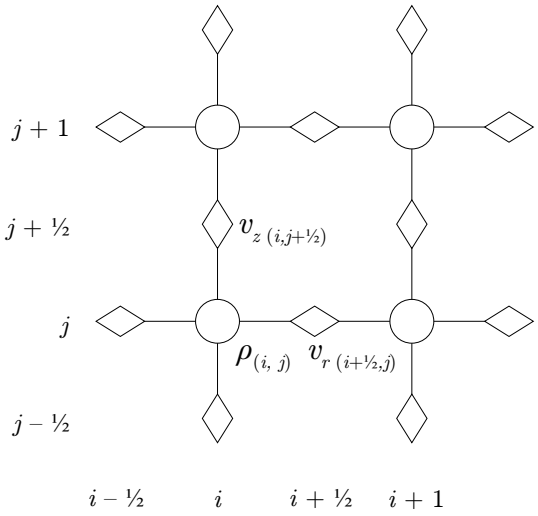


Figure 7.1: Spatial discretization as in standard acoustics FDTD method. The pressure ($p^m_{i,j}$) and the n-th order relaxation process state fields ($S^m_{n,i,j}$) are evaluated at same discrete location as the density ($\rho^m_{i,j}$). Particle velocity fields are discretized staggered in both space and time respect to the density, pressure and the n-th order state fields.

correct the numerical dispersion and include artificial attenuation to guarantee convergence in nonlinear regime. Moreover the inclusion of relaxation processes in the presented formulation require only one extra field per relaxation process and no memory buffer is needed.

7.3.1 Discretization

Cylindrical axisymmetric $\mathbf{x} = (r, z)$ coordinate system is considered in this work, however, the method can be derived in other coordinate system. As in the standard acoustic FDTD method (Botteldooren, 1996), the particle velocity fields are discretized staggered in time and space respect to the density and pressure fields. As shown in Fig. 7.1 uniform grid is considered, where $r = i\Delta r$, $z = j\Delta z$, $t = m\Delta t$, with Δr and Δz as the radial and axial spatial steps, and Δt is the temporal step.

Centered finite differences operators are applied over the partial derivatives of the governing equations. Thus, spatial interpolation is needed over the off-center grid variables in order to fulfill the conservation principles over each discrete cell of the domain (LeVeque, 1992). The r component of Eq. (7.2) is expressed in a

cylindrical axisymmetric system as

$$\begin{aligned}\frac{\partial v_r}{\partial t} =& -\frac{1}{\rho}\frac{\partial p}{\partial r} - v_r\frac{\partial v_r}{\partial r} - v_z\frac{\partial v_r}{\partial z} \\ &+ \frac{\eta}{\rho}\left(\frac{\partial^2 v_r}{\partial r^2} + \frac{1}{r}\frac{\partial v_r}{\partial r} + \frac{\partial^2 v_r}{\partial z^2} - \frac{v_r}{r^2}\right) \\ &+ \frac{1}{\rho}\left(\zeta + \frac{1}{3}\eta\right)\left(\frac{\partial^2 v_r}{\partial r^2} + \frac{1}{r}\frac{\partial v_r}{\partial r} + \frac{\partial^2 v_z}{\partial r \partial z} - \frac{v_r}{r^2}\right).\end{aligned} \tag{7.20}$$

Each term of the above expression is approximated by centered finite differences evaluated at $r = (i + \frac{1}{2}) \cdot \Delta r$, $z = (j + \frac{1}{2}) \cdot \Delta z$, $t = (m + \frac{1}{2}) \cdot \Delta t$. This equation can be solved obtaining an update equation for $v_{r_{i+\frac{1}{2},j}}^{m+\frac{1}{2}}$. In the same way, the z component of the motion equation (7.2) is expressed as

$$\begin{aligned}\frac{\partial v_z}{\partial t} =& -\frac{1}{\rho}\frac{\partial p}{\partial z} - v_r\frac{\partial v_z}{\partial r} - v_z\frac{\partial v_z}{\partial z} \\ &+ \frac{\eta}{\rho}\left(\frac{\partial^2 v_z}{\partial r^2} + \frac{1}{r}\frac{\partial v_z}{\partial r} + \frac{\partial^2 v_z}{\partial z^2}\right) \\ &+ \frac{1}{\rho}\left(\zeta + \frac{1}{3}\eta\right)\left(\frac{\partial^2 v_r}{\partial z \partial r} + \frac{1}{r}\frac{\partial v_r}{\partial z} + \frac{\partial^2 v_z}{\partial z^2}\right).\end{aligned} \tag{7.21}$$

This equation is approximated by centered finite differences and evaluated at $r = i \cdot \Delta r$, $z = (j + \frac{1}{2}) \cdot \Delta z$, $t = m \cdot \Delta t$. An update equation is obtained solving this equation for $v_{z_{i,j+\frac{1}{2}}}^{m+\frac{1}{2}}$. The equation (7.1) in cylindrical axisymmetric coordinate system is expressed as

$$\frac{\partial \rho}{\partial t} = -\rho\left(\frac{\partial v_r}{\partial r} + \frac{v_r}{r} + \frac{\partial v_z}{\partial z}\right) - v_r\frac{\partial \rho}{\partial r} - v_z\frac{\partial \rho}{\partial z}. \tag{7.22}$$

Following the same procedure, each term of the above expression is approximated by centered finite differences and evaluated at $r = i \cdot \Delta r$, $z = j \cdot \Delta z$, $t = (m + \frac{1}{2}) \cdot \Delta t$, and the update equation is obtained solving this expression for $\rho_{i,j}^{m+1}$.

A leap-frog time marching is applied to solve Eq. (7.20-7.22) for each time step until the desired simulation time is reached. Finally, Eq. (7.8) is locally solved for $m + 1$ by and explicit fourth-order Runge-Kutta method and then Eq. (7.10) is evaluated.

7.3.2 Boundary conditions

The staggered grid is terminated on velocity nodes, so the boundary conditions are applied on these external nodes, allowing to prevent the singularity of the cylindrical coordinate system: due to the staggered grid, the only variable discretized at

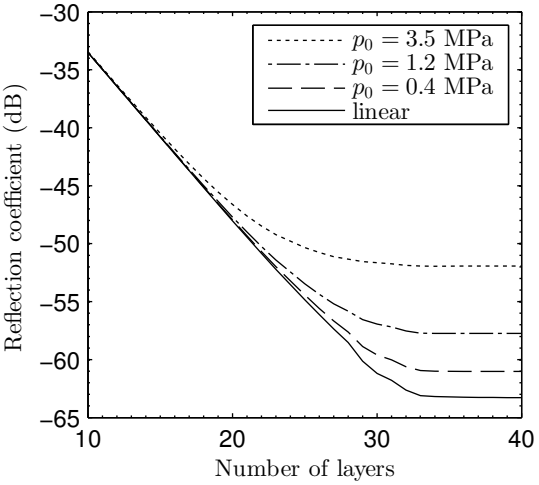


Figure 7.2: Reflection coefficient of the perfectly matched layer (PML) versus number of layers for different wave amplitudes.

$r = 0$ is v_r, and axisymmetric condition $v_r|_{r=0} = 0$ is applied there. Furthermore, to solve spatial differential operators at boundaries some "ghost" nodes must be created with the conditions: $v_r(-r) = -v_r(r)$, $v_z(-r) = v_z(r)$, $\rho(-r) = \rho(r)$ and $p(-r) = p(r)$.

Perfectly matched layers (PML) (Liu et al., 1997) were placed in the limits of the domain ($\pm z$ and $+r$) to avoid spurious reflections from the limits of the integration domain. Inside the PML domains linearized acoustic equations were solved using the complex coordinate screeching formulation (Liu, 1999). For a layer of 30 elements and a broadband incident wave with 1 MHz central frequency and non-normal incidence angle, these absorbent boundary conditions have reported a reflection coefficient of $R = -55.2$ dB.

However, the performance of the PML is amplitude dependent as long the nonlinear terms are uncoupled to the PML domains. The amplitude dependence of the reflection coefficient is shown in Fig. 7.2, where a PML of 25 elements thickness have reported reflection coefficients $R < -50$ dB for waves in linear regime and highly nonlinear waves including shocks.

7.3.3 Minimizing numerical dispersion

The stability for the lossless linear FDTD algorithm follows the Courant-Friedrich-Levy (CFL) condition, that for uniform grid ($\Delta r = \Delta z = \Delta h$) the maximum duration of the time step is limited by $\Delta t \leq \Delta h / c_0 \sqrt{D}$ where D is the number of dimensions (i.e. $D = 2$ in cylindrical axisymmetric coordinate system). That

condition essentially states that for a single time step information can not propagate in the numerical grid a distance longer that one cell. However, if relaxation is included numerical instabilities have been observed when $\tau_f/2\pi < \Delta t$. Due to this empirical relation, the maximum values for relaxation frequencies are limited too by the chosen spatial discretization by the simple relation $f_n < \sqrt{2}N_\lambda f_0$, where $f_n = 2\pi/\tau_n$ is the maximum relaxation frequency for all processes, N_λ is the number of spatial samples per wavelength and f_0 the frequency of the propagating wave.

On the other hand, nonlinear effects induce the progressively growing of harmonics of the fundamental frequency of the initial wave. The diffusive viscous terms in Eq. (7.2), attenuates the small-amplitude high-spatial frequencies, damping the "node to node" numerical oscillations and ensuring numerical stability in weakly nonlinear regime. Thus, for a smooth solution the numerical algorithm shows consistency when $\Delta h \to 0$, so if stability is achieved by the CFL condition, the convergence is guaranteed. However, in strongly nonlinear regime, i.e. when sharp waveforms or even shocks are present in the solution, extra numerical techniques must be employed to guarantee convergence. Artificial viscosity can be added when shock waves are present in the solution where a common implementation follows a fourth order spatial filtering (Sparrow et al., 1991; Ginter et al., 2002). Thus, the artificial attenuation retrieved by this spatial operator is fourth power of frequency: the low frequency components of the solution remains quasi-undamped, while the higher spatial frequencies are strongly attenuated. In this way, the solution is smoothed and shock thickness depends on the artificial viscosity coefficient.

However, the main drawback for finite difference methods is numerical dispersion, where the analytic dispersion relation can be expressed in 1D as

$$\sin^2 \frac{k\Delta h}{2} = \frac{1}{S^2} \sin^2 \frac{\omega \Delta t}{2}, \tag{7.23}$$

with the Courant number $S = c_0\Delta t/\Delta h$. In this way, numerical dispersion reduces phase speed for high frequency components so traveling sharp solutions develop tail oscillations: the low wavenumbers travels fast and left behind high spatial frequencies. In nonlinear regime, is well-known that the combined effects of nonlinearity and strong dispersion can lead rich phenomena, e.g. beatings in the generated harmonics, pulsations on the vertex of a sawtooth wave or soliton formation in strong dispersive media (Rudenko et al., 1977). In this way, the numerical dispersion by discreteness of the FDTD methods couple to the physical nonlinearity can lead to a great variety of non-physical or even unstable solutions.

In order to overcome those two limitations, i.e. the generation of harmonics over the discrete limit and the numerical dispersion, we propose the use of artificial relaxation. Physical relaxation processes introduces *anomalous* dispersion, i.e. the phase speed increases in the high frequency regime, opposite to the numerical (lattice) dispersion described above. Thus, by introducing a collection of

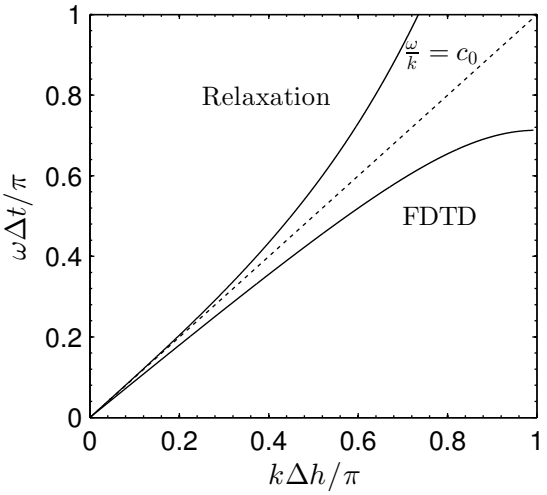


Figure 7.3: Normalized dispersion relation for of a FDTD lattice of Courant number $S = 0.9$ and *anomalous* dispersion relation for a mono relaxing acoustic media. The straight line $c_0 = \omega/k$ represents the reference nondispersive case.

relaxation processes and choosing its adequate relaxation parameters the high frequency numerical dispersion can be compensated. As a consequence, introduction of those relaxation processes in the high frequency lead to the inevitable inclusion of artificial attenuation. However, this numerical attenuation is then exploited to limit the growing of higher harmonics in a similar way than artificial viscosity (Sparrow et al., 1991). It is worth noting here that, due to the attenuation using artificial relaxation is, at maximum, only second power of frequency, the low frequency range of the solution is therefore also attenuated. Thus, the proposed method is restricted to lossy media.

The adequate relaxation parameters that corrects the numerical dispersion have been found by multi-objective optimization techniques, where two cost function are proposed: one for dispersion and other for attenuation. In the first case, the error between the goal (ideal) dispersion relation and the retrieved numerical dispersion corrected by multiple artificial relaxation and is evaluated in the high frequency regime. Finally, the second cost function is the error between the desired (ideal) attenuation and the artificial attenuation evaluated in the low frequency regime.

7.4 Validation

7.4.1 Single relaxation process

A canonical case of a physical single relaxation process is presented. In order to correct numerical dispersion the parameters of two extra artificial relaxation processes have been found using the multi-objective genetic algorithms provided by the optimization toolbox in MATLAB R2014a v8.03. Linear propagation was considered and simulation parameters were set to typical values for water: $c_0 = 1500$ m/s, $\rho_0 = 1000$ kg/m^3, $B/A = 5$, $\eta = 8.90 \cdot 10^{-4}$ Pa·s. A single physical relaxation process was included, with a characteristic relaxation time of $\tau_1 = 1/2\pi f_0$ and $f_0 = 2$ MHz, and relaxation modulus of $\eta_1 = 0.0134$ that leads to a frozen sound speed of $c_\infty = 1510$ m/s. In this case, the numerical parameters were set to $\Delta r = \Delta z = 1.87 \cdot 10^{-7}$ m and $\Delta t = 8.65 \cdot 10^{-11}$ s. A plane wave traveling in $+z$ direction was considered.

Thus, the theoretical attenuation for the relaxation processes and including viscosity can be expressed as

$$\alpha(\omega) = \frac{\omega^2}{2\rho_0 c_0^3}\left(\zeta + \frac{4}{3}\eta\right) + \sum_{n=1}^{N} \frac{\eta_n}{2c_0\tau_n}\frac{\omega^2\tau_n^2}{1+\omega^2\tau_n^2}, \tag{7.24}$$

and the theoretical phase velocity can be predicted as (Pierce, 1989)

$$c_p(\omega) = c_0\left(1 + \sum_{n=1}^{N} \frac{\eta_n}{2}\frac{\omega^2\tau_n^2}{1+\omega^2\tau_n^2}\right). \tag{7.25}$$

In order to compute the attenuation and dispersion of the numerical method, simulated pressure was recorded at two locations z_0 and z_1, and attenuation and phase velocity were estimated from the spectral components over the bandwidth of the input signal. The numerical attenuation was calculated as

$$\alpha(\omega)_{fd} = \frac{\ln\left(|P(\omega, z_1)/P(\omega, z_0)|\right)}{(z_1 - z_0)}, \tag{7.26}$$

where $P(\omega)$ is the Fourier transform of the measured pressure waveforms at points z_0 and z_1. On the other hand, the phase velocity was computed as

$$c_p(\omega)_{fd} = \frac{\omega \cdot (z_1 - z_0)}{\arg\left(P(\omega, z_1)/P(\omega, z_0)\right)}, \tag{7.27}$$

where correct phase unwrapping is needed.

In this way, Fig. 7.4 shows the retrieved Pareto front of the optimization, where 3 different areas can be distinguished. The first area, marked as (A) in Fig. 7.4, represents individuals those numerical dispersion is minimal but attenuation is not optimal. On the other hand, the individuals around area (B) represent a set of relaxation parameters that provides the best agreement between numerical and physical attenuation. A good compromise between both situations can be obtained in the central area of the Pareto front (C), where retrieved attenuation and dispersion in the low frequency band shows good agreement with the physical, and the numerical dispersion has been corrected over a wide frequency range. However, as can be seen in the inset of Fig. 7.4, the dispersion relation retrieved by all the cases corrects the FDTD lossless numerical dispersion relation. The phase speed of those tree individuals is shown in Fig. 7.5 b), where it can be seen that in the frequency range selected for the optimization the numerical phase speed is corrected for all the individuals, where the best fit is obtained for individuals in the Pareto front area A. On the other hand, the inclusion of artificial relaxation leads to an increasing of the attenuation in the high frequency range, as is shown in Fig. 7.5 a). In this way, as the phase speed error is reduced the effect of artificial attenuation increases. Although this increasing can be seen as a non-desired counterpart, the appearance of this attenuation is useful in order to control the harmonic growing in nonlinear regime in the same way as artificial viscosity

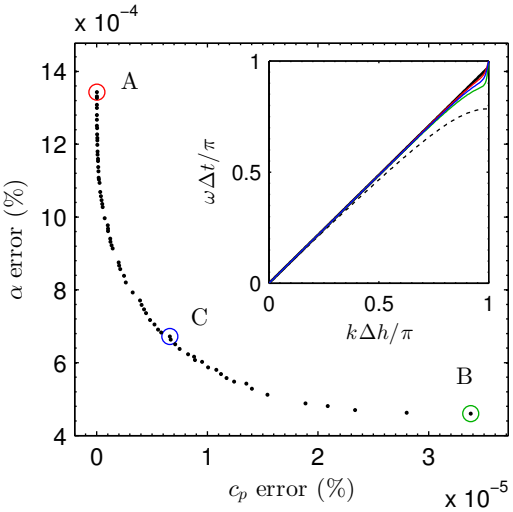


Figure 7.4: Pareto front retrieved by the multi-objective genetic optimization. Red marker (A) is the solution those relaxation parameters minimizes the numerical dispersion. The best fit in the attenuation are the parameters that provided the solution marked by green circle (B). A compromise between attenuation and dispersion is achieved at the individuals in the center of the Pareto front as the sample marked by blue circle (C). The inset shows the normalized dispersion relation retrieved by the individuals A-C. Dashed black line shows the numerical dispersion relation of the FDTD method for a Courant number of 0.94 without artificial relaxation.

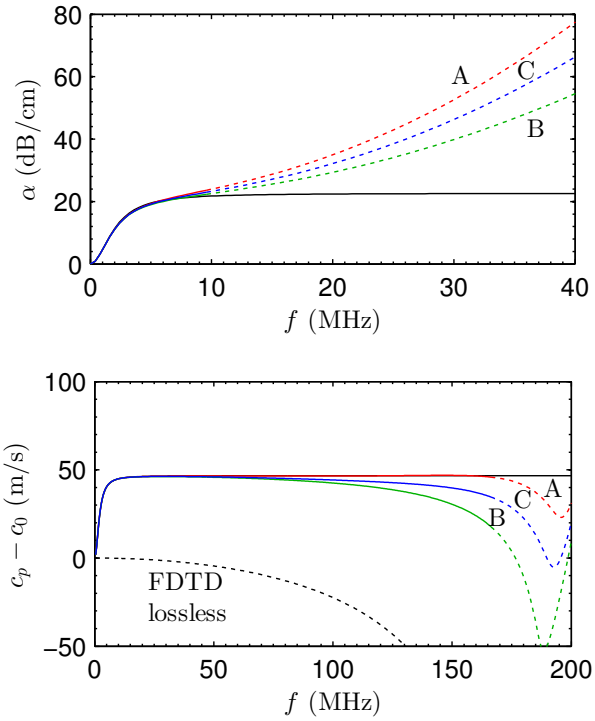


Figure 7.5: Retrieved attenuation (Up) and dispersion (Down) by the inclusion of artificial relaxation for the individuals A (red), B (green) and C (blue) of Fig. 7.4. Continuous lines represent the frequency range included by the optimization and dashed lines the not useful frequency range. As a consequence of correcting dispersion appears attenuation in the high frequency range that will be used as artificial attenuation for nonlinear stability.

spatial operators (Sparrow et al., 1991).

7.4.2 Nonlinear steady solution for single relaxation process

In order to validate the method in the nonlinear regime a full-wave simulation was developed in a mono-relaxing media using above parameters. Thus, the analytical (inverted) solution for the steady solution with $p = -p_0$ for $\tau = -\infty$, $p = p_0$ for $\tau = \infty$ and $p = 0$ for $\tau = 0$, for the retarded time $\tau = t - z/c_0$ reads (Hamilton et al., 1998b)

$$\tau = \tau_n \ln \frac{(1 + p/p_0)^{D-1}}{(1 - p/p_0)^{D+1}} \tag{7.28}$$

where $D = \eta_n \rho_0 c_0^2 / 2\beta p_0$ measures the ratio of relaxation effects to nonlinear effects.

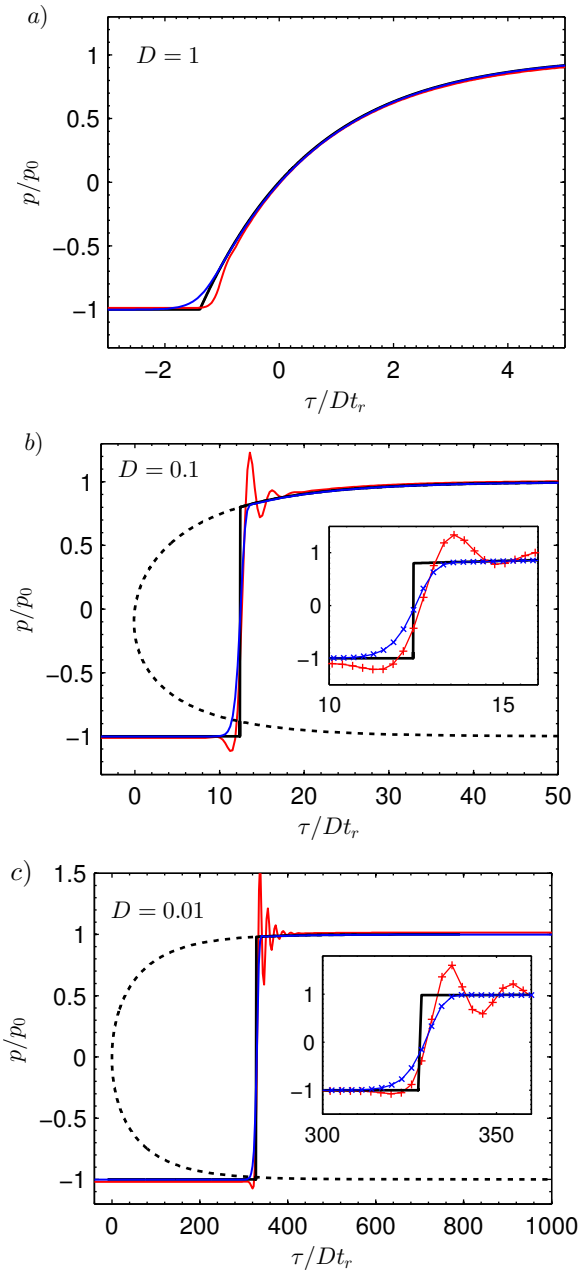


Figure 7.6: a) Analytical (gray line), numerical using artificial relaxation with corrected dispersion (blue line) and artificial viscosity (red) (Sparrow et al., 1991) for the nonlinear steady state solution for D=1. b) Nonlinear steady state solution for D=0.1. Inset shows detailed shock numerical solution for artificial relaxation (blue) and artificial viscosity (red). c) Nonlinear steady state solution for D=0.01.

For $D > 1$, where no shock is present, the solution retrieved by FDTD algorithm shows good agreement with analytical and no artificial relaxation is needed. However, for $D < 1$ a discontinuity is present in the solution and convergence is only possible with the inclusion of extra numerical techniques.

Thus, Fig. 7.6 (a-c) shows the analytical and numerical solutions including artificial relaxation and artificial viscosity, where excellent agreement is achieved in all cases. In the case of artificial viscosity, higher harmonics are strongly attenuated and by reducing grid step convergence can be achieved. However, as long the phase speed of the higher spatial frequencies present in the shock is modified due to numerical dispersion, oscillations appears in the tail of the discontinuity, leading to the appearance of non-physical solutions. On the other hand, the artificial attenuation by relaxation also limits the harmonic growing so a smooth version of the shock appears. Moreover, artificial relaxation also corrects phase velocity so all the spatial frequencies travels at same speed and no oscillatory tail appears. The case of $D = 0.01$ is shown in Fig. 7.6 c), where nonlinear effects strongly dominates over attenuation. In this case, tail oscillations provided by artificial viscosity increases in amplitude. In contrast, by including artificial relaxation a smoothed version of the shock is captured and accuracy is maintained.

7.5 Results

7.5.1 Frequency power law attenuation

Using methodology described above, the optimal relaxation parameters were obtained in order to fit the multiple-relaxation numerical attenuation to frequency power law attenuation in the form

$$\alpha(\omega) = \alpha_0 \omega^{\gamma}, \tag{7.29}$$

where γ is the power law exponent and α_0 the power law coefficient in Np $(\mathrm{rad/s})^{\gamma}\mathrm{m}^{-1}$. Moreover, the numerical dispersion was corrected by means of artificial relaxation in order to fit the corresponding frequency power law dispersion, where its analytical form satisfying causality can be expressed as (Waters et al., 2005)

$$\frac{1}{c_p\left(\omega\right)} = \frac{1}{c(\omega_0)} + \alpha_0 \tan\left(\frac{\pi\gamma}{2}\right)\left(|\omega|^{\gamma-1} - |\omega_0|^{\gamma-1}\right). \tag{7.30}$$

This expression is valid for $0 < \gamma < 3$ with $\gamma \neq 1$, and an alternate equation can be found (Waters et al., 2005) in the limit for $\gamma = 1$. Here, simulation parameters were $c_0 = 1500$ m/s, $\rho_0 = 1000$ kg/m^3, $B/A = 5$, $\eta = 8.90 \cdot 10^{-4}$ Pa·s, $f_0 = 1$ MHz, $\Delta r = \Delta z = 1.3 \cdot 10^{-5}$ m, $\Delta t = 5.4 \cdot 10^{-9}$ s; that leads to 26 elements per wavelength and a CFL number of 0.9. Only two independent relaxation processes were employed in this section to obtain the target frequency power laws.

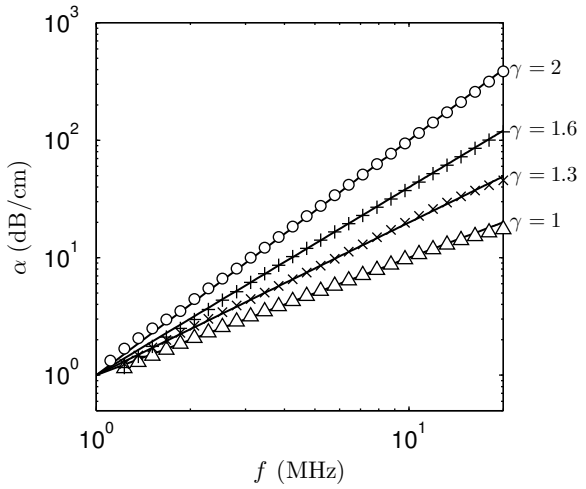


Figure 7.7: Attenuation retrieved by the numerical algorithm (markers) and target frequency power law attenuation (gray lines). By using the optimization algorithm the relaxation times and modulus were optimized for minimize the relative error between the target power laws of $\gamma = [1, 1.3, 1.6, 2]$ and the attenuation retrieved.

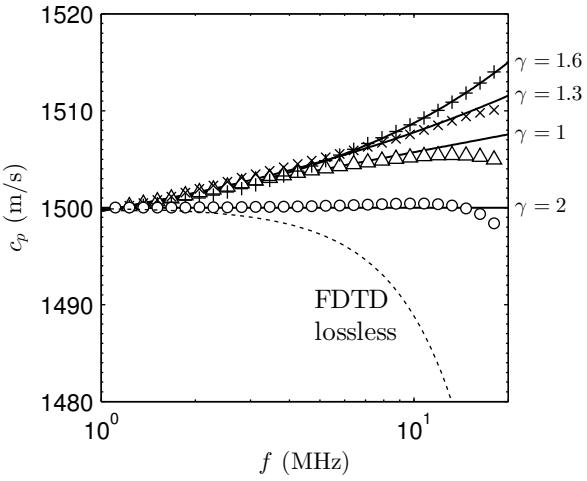


Figure 7.8: Phase speed retrieved by the numerical algorithm (markers) and target frequency power law attenuation (gray lines) for $\gamma = [1, 1.3, 1.6, 2]$.

Following the above procedure, the relaxation times τ_n and relaxation modulus η_n were optimized for different frequency power laws covering the range of that observed in tissues $\gamma = [1, 1.3, 1.6, 2]$. The attenuation coefficient α_0 was chosen for each power law to present an attenuation $\alpha = 1$ dB/cm/MHz$^\gamma$. The fitting was developed over the typical frequency range for medical ultrasound applications,

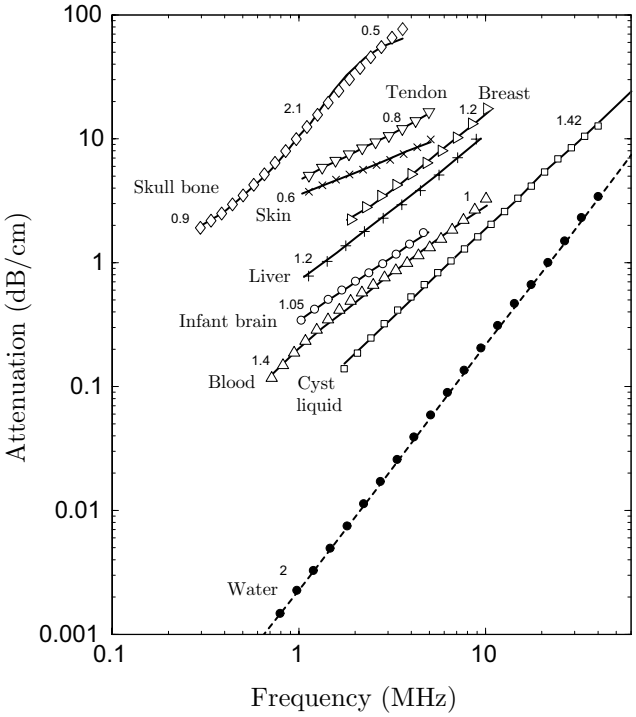


Figure 7.9: Experimental attenuation data for some tissues adapted from (Hill et al., 2004) (lines), and obtained by the numerical method (markers) by fitting the parameters of 2 relaxing processes. The numbers above the curves show the coefficient of the frequency power law γ for each frequency region (i.e. the slope of the curve).

i. e. 1 to 20 MHz for both attenuation and phase speed. The results for the attenuation and phase speed curves are plotted in Fig. 7.7 and Fig. 7.8, where the theoretical and the numerical predictions agree over the frequency range used for the fitting.

7.5.2 Fitting attenuation for tissue experimental data

Although a frequency power law dependence can describe the ultrasound attenuation over a finite frequency range, the attenuation data of some particular examples shows variation of the exponent over the entire frequency range (Hill et al., 2004). Thus, Fig. 7.9 shows experimental attenuation data curves for some tissues where the local slope of the power law changes over the measured frequency range. This behavior can be modeled by a sum of relaxation processes by optimizing the relaxation parameters as described above. Thus, the results show that most tissues

Table 7.1: Error of the optimized attenuation response relative to the experimental data for N relaxation processes.

Tissue	Power law (local slope)	$N = 1$ $\varepsilon(\%)$	$N = 2$ $\varepsilon(\%)$	$N = 3$ $\varepsilon(\%)$	$N = 4$ $\varepsilon(\%)$
Skin	$f^{0.6}$	6.67	0.167	0.136	0.120
Liver	$f^{1.2}$	7.62	0.517	0.404	0.165
Blood	$f^{1.4}$, f^{1}	8.34	0.349	0.330	0.310
Breast	$f^{0.9}$, $f^{1.2}$	5.20	0.216	0.209	0.205
Skull bone	$f^{0.9}$, $f^{2.1}$, $f^{0.5}$	10.60	10.54	8.628	5.189

with locally variable γ can be fitted by only a pair of relaxation processes, as the same way that for constant-slope frequency power law attenuation (Cleveland et al., 1996).

In this way, Table 7.1 shows the error of the numerical attenuation relative to the experimental data. The percent relative error was computed as

$$\varepsilon = \frac{100}{f_2 - f_1} \int_{f_1}^{f_2} \frac{|\alpha_e(f) - \alpha(f)|}{\alpha_e(f)} \, \mathrm{d}f, \tag{7.31}$$

where $\alpha_e(f)$ is the experimental attenuation data, f_1 and f_2 define the frequency range of the measurement.

As expected, the goodness of fit grows as the number of relaxation processes included increases. However, only two processes are enough to obtain relative errors below 1% for tissues with $\gamma < 2$. In the case of tissues where a local value of $\gamma > 2$ has been observed, the fitting procedure fails, like in the skull bone in the 2 MHz range (Hill et al., 2004). The maximum slope achieved by single relaxation and thermo-viscous losses is $\gamma = 2$ for any frequency, so a tissue showing that slope cannot be accurately modeled in this frequency region with the method proposed in this work. Another point of view of is from dispersion: Eq. (7.30 states that frequency power law medium with $2 < \gamma < 3$ presents standard dispersion (Waters et al., 2005), opposite to *anomalous* dispersion for media falling in the range $0 < \gamma < 2$. Therefore, the dispersion relation of media with $2 < \gamma < 3$ cannot be modeled by a sum of relaxation processes as long relaxation includes *anomalous* dispersion.

Using Kramers-Kronig relationships (O'Donnell et al., 1981), the variations of sound speed Δc can be predicted by the frequency dependent attenuation. Table 7.2 shows the variation of sound speed observed in the numerical solution over the fitted frequency range. The magnitude of these variations are of the order of magnitude of those measured experimentally in this frequency range, and the frequency dependence observed for the variation is roughly linear as observed in real

Table 7.2: Variation of sound speed (Δc) observed numerically for the modeled tissues by means of two relaxation processes and analytical using the Kramers-Kronig relations.

Tissue	Numerical Δc (m/s)	Analytical Δc (m/s)
Skull bone	80.737	70.720
Skin	10.148	2.460
Breast	2.323	2.455
Liver	3.118	2.339
Blood	0.865	0.907

tissue (Hill et al., 2004). As expected from the relations between dispersion and absorption (O'Donnell et al., 1981), the magnitude of the variation in sound speed increases as the total variation of the absorption increases for a given frequency range.

7.5.3 Nonlinear one-dimensional propagation in tissue-like media

Non-dispersive media

In order to study the convergence of the numerical calculations to an analytical solution of the model in the nonlinear regime, a medium with frequency squared dependence attenuation is implemented using the adequate relaxation times and relaxation modulus as explained above. The solution for the frequency squared absorption is compared with the analytical solution for a plane wave traveling through a thermo-viscous fluid proposed by Mendousse (Pierce, 1989):

$$\frac{p}{p_0} = \frac{\frac{4}{\Gamma}\sum_{n=1}^{\infty}(-1)^{n+1} I_n\left(\frac{\Gamma}{2}\right) n\mathrm{e}^{-n^2\sigma/\Gamma}\sin\left(n\omega t'\right)}{I_0\left(\frac{\Gamma}{2}\right) + 2\sum_{n=1}^{\infty}(-1)^{n} I_n\left(\frac{\Gamma}{2}\right) n\mathrm{e}^{-n^2\sigma/\Gamma}\cos\left(n\omega t'\right)} \tag{7.32}$$

where Γ is the Gol'dberg number, defined for power law media as $\Gamma = x_a/x_s$, with absorption length $x_a = 1/\alpha_0\omega^{\gamma}$, shock formation distance $x_s = 1/\beta\varepsilon k$ and normalized distance $\sigma = x/x_s$; with the parameter of nonlinearity $\beta = 1 + B/2A$ and the acoustic Mach number $\varepsilon = v/c_0$, with v is the source particle velocity and k the wavenumber.

Figure 7.11 (top) present the simulated waveforms at $\sigma = 1$ and $\sigma = 3$. The wave steepening due to nonlinear processes in the absence of dispersion are well resolved by the numerical method presented here. In order to study the accuracy of the algorithm, the amplitude of the first ten harmonics has been extracted for numerical and analytic solutions and plotted versus σ in Fig. 7.11 (bottom). The

observed relative error of the computational method decreases due to grid coarsening by a square law (i.e. the numerical scheme is second order accuracy). The magnitude of the error mainly depends on the number of elements per wavelength but, due to not ideal dispersion, also on the traveled propagated distance. Including the correction of dispersion by artificial relaxation, for a path length of 100 λ, a grid of 26 elements per wavelength was needed to obtain a relative error below 1 % for the third harmonic. Obviously, the relative error of the first and second harmonics will be always lower, i.e. the fundamental component error was 0.072 %.

In addition, the solution was compared also to the obtained by a k-space method applied to the constitutive relations by using the k-wave algorithm (Treeby et al., 2012). This method was selected due to the low numerical dispersion and the possibility of including frequency power law attenuation. The result of both computational methods and Eq. (7.32) agree over all the spectral components analyzed, showing convergence to the analytic solution.

Dispersive media

In the case of frequency power law attenuation media with $\gamma \approx 1$ no general analytic solution exist in nonlinear regime for monochromatic progressive waves. Thus, in order to study convergence in this regime, the proposed FDTD solution was compared with the solution obtained by k-space methods (Treeby et al., 2012). By using same physical and grid parameters in both methods, the solutions agrees for different power laws. Thus, Fig. 7.12 (top) shows the good agreement for the waveforms measured at $\sigma = 1$ and $\sigma = 3$ obtained for $\gamma = 1.6$, where the characteristic asymmetry of media with *anomalous* dispersion (e.g. relaxing, boundary layer effects) (Hamilton et al., 1998b) is observed: the shock front after the rarefaction phase is followed by a rounded positive compression profile. The spatial distribution for each harmonic is shown in Fig. 7.13 (bottom), where it is observed that the proposed FDTD solution with optimized attenuation and dispersion converges to the obtained by pseudo-spectral methods up to ten harmonics. As in the case of frequency squared media, grid refinement numerical tests have reported a second order accuracy of the FDTD method in nonlinear regime.

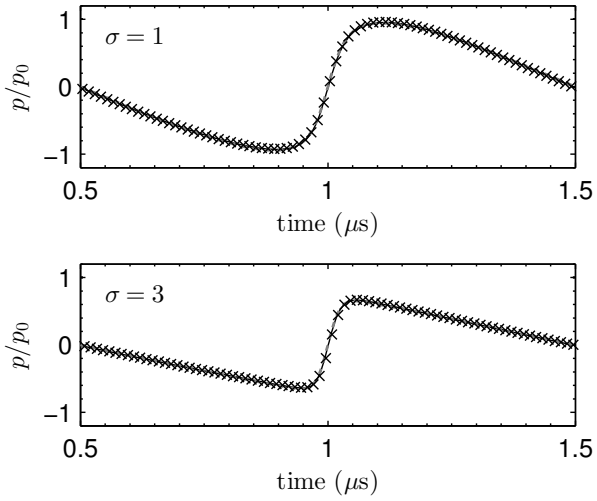


Figure 7.10: Waveforms for $\sigma = 1$ and $\sigma = 3$ in a media with frequency squared power law. Mendousse analytical solution (blue line), k-space numerical solution (gray line) and FDTD numerical solution (markers).

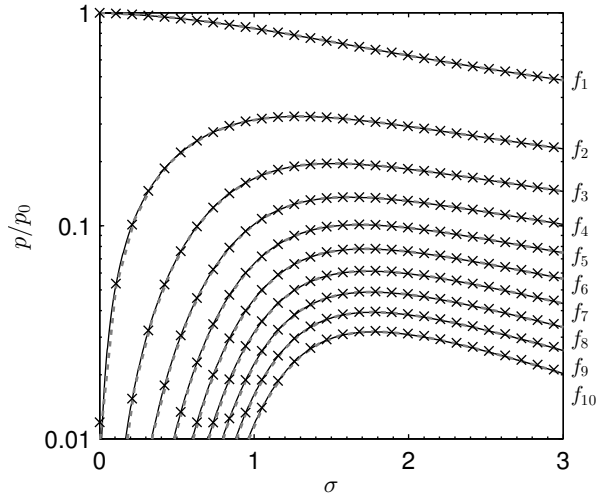


Figure 7.11: Spatial distribution of the first ten harmonics for $\gamma = 2$. Mendousse analytical solution (blue line), k-space numerical solution (gray line) and FDTD numerical solution (markers).

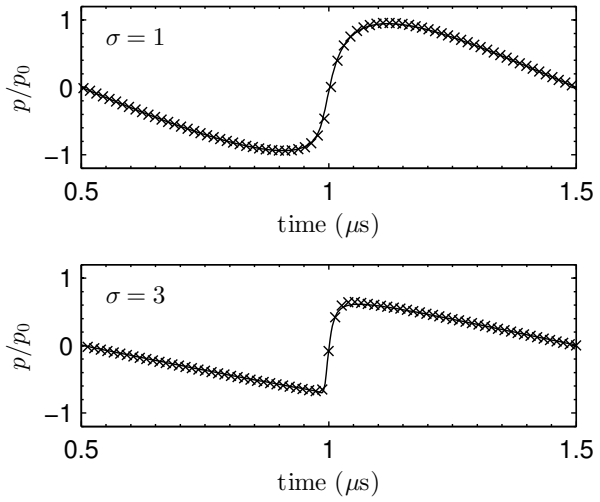


Figure 7.12: Waveforms for $\sigma = 1$ and $\sigma = 3$ in a media with frequency power law ($\gamma = 1.6$). k-space numerical solution (gray line) and FDTD numerical solution (markers).

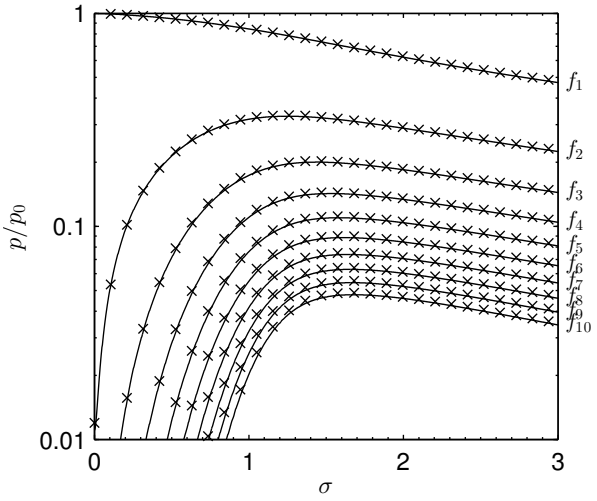


Figure 7.13: Spatial distribution of the first ten harmonics for $\gamma = 1.6$. k-space numerical solution (gray line) and FDTD numerical solution (markers).

7.5.4 Nonlinear propagation in tissue-like media including diffraction

Experimental validation

An experiment was designed to test the validity of the algorithm for intense beams in frequency power law attenuation media. The source was formed by a plane single element piezoceramic crystal (PZ 26, Ferroperm Piezoceramics, Denmark) mounted in a custom designed steel housing and a Polymethyl methacrylate (PMMA) focusing lens with aperture $A = 50$ mm and radius of curvature $R = 50$ mm. The source was driven with a sinusoidal pulse burst of frequency $f_0 = 1.112$ MHz and $n = 50$ cycles using a function generator (14 bits, 100 MS/s, model PXI5412, National Instruments) and a linear RF amplifier (ENI 1040L, 400W, 55dB, ENI, Rochester, NY). The pressure waveforms were acquired with a HNR 500 μm needle PVDF hydrophone (Onda Corp, CA), and a digitizer (64 MS/s, model PXI5620, National Instruments) were used. A three-axis micropositioning system (OWIS GmbH, Germany) was used to move the hydrophone in three orthogonal directions with an accuracy of 10 μm and a National Instruments PXI-Technology controller NI8176 was used to control all the devices. The amplitude frequency response of the hydrophone was compensated in post-processing but not in phase due to the absence of phase calibration for this equipment. A scheme of the measurement setup is shown in Fig. 7.14.

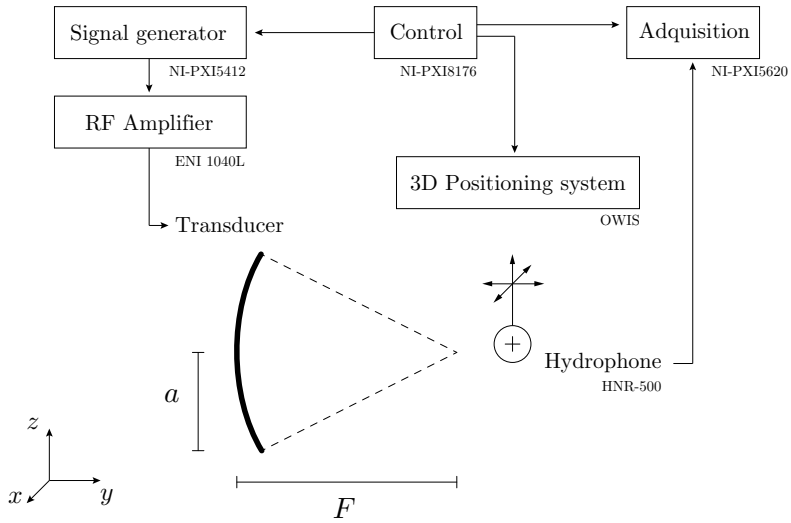


Figure 7.14: Scheme of the measurement system

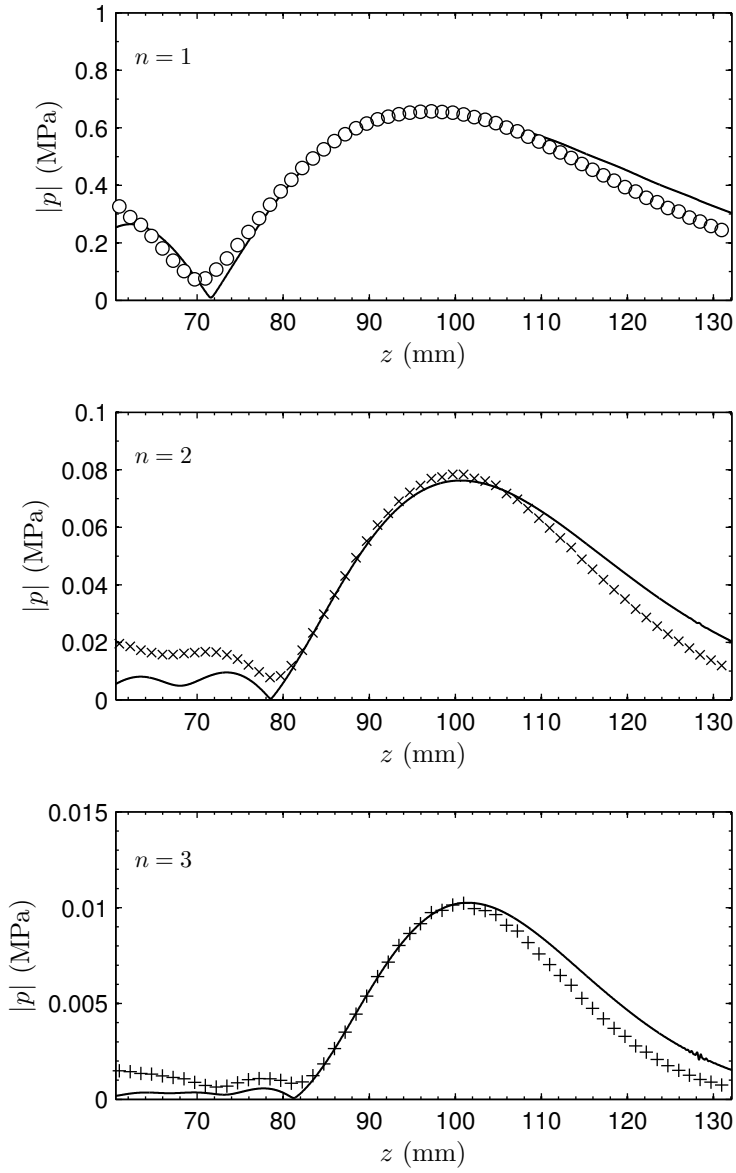


Figure 7.15: Spatial distribution of the fundamental (o), second ($\times$) and third ($+$) harmonics obtained by the numerical (continuous line) and experimental methods (markers) for a focused transducer immersed in castor oil.

The source was completely immersed in a castor oil tank ($350 \times 350 \times 350$ mm). We select this frequency power law attenuation media due to the low variability of its acoustic properties along existent literature (Liebler et al., 2004; Treeby et al., 2009). Using a sound speed inside the bulk of the lens $c_l = 2711$ m/s, and a sound speed of the castor oil of $c_0 = 1480$ m/s (at 26º C room temperature), the effective lens geometrical focal is estimated as $F = R/(1 - c_0/c_l) = 110.1$ mm, leading to a linear lossless gain of $G = 13.4$.

On the other hand, a nonlinear simulation including diffraction and frequency power law attenuation with same parameters was carried out in a workstation (20 cores Intel Xeon E5-2680 CPU, 2.8GHz with 256 GB RAM). The boundary conditions were implemented for a spherical focused ultrasound source. The castor oil parameters at 26º C room temperature (Treeby et al., 2009), were $c_0 = 1480$ m/s, $\rho_0 = 961$ kg/m^3, $\alpha = 0.4$ dB/cm/MHz$^\gamma$, $\gamma = 1.69$, $B/A = 12.0$. The grid parameters were $\Delta r = \Delta z = 29.6$ μm and $\Delta t = 13.6$ ns, leading to a CFL number $S = 0.95$ and $N_\lambda = 50$ elements per wavelength at fundamental frequency, note that this grid leads to $N_\lambda = 16$ for third harmonic.

The balance between nonlinear effects and power law attenuation can be estimated by using the Gol'dberg ratio, $\Gamma = x_a/x_s$ where x_s is the shock formation distance and x_a the media attenuation characteristic length. Thus, the amplitude of the source were selected to obtain a Gol'dberg ratio of $\Gamma = 0.25$ in order to let the frequency power law attenuation effects slightly dominate over nonlinear effects. On the other hand, the ratio between diffraction effects and nonlinear effects can be described by the so called Khokhlov number $N = x_d/x_s$, where $x_d = ka^2/2$ is the diffraction length and a source radius. For the proposed test a Khokhlov number of $N = 0.49$ was selected to let the nonlinear effect slightly dominate over diffraction effects. The selected excitation pressure amplitude was $p_0 = 87.7$ kPa.

The results are summarized in Fig. 7.15, where axial pressure distribution for the fundamental, second and third harmonic are presented. A good agreement is found between simulations and the experimental test. Only far to the focal point the amplitude there exist differences between computations and experiments, that can be caused by nonuniform vibration of the source (Canney et al., 2008), boundary effects of the PMMA lens, or miss-alignment of the source axis and micropositioning system orthogonal directions along the 100 mm axial measurement.

The maximum amplitudes of the first harmonic were $p_{e1} = 0.6539$ MPa for the experiment and $p_{n1} = 0.6576$ for the numeric. The second harmonic peak pressure was $p_{e2} = 78.368$ kPa and $p_{n2} = 76.272$ kPa, and the third harmonic peak pressure $p_{e3} = 10.146$ and $p_{n3} = 10.252$ kPa for the experimental and numeric respectively. The relative errors between numerical and experimental results are 0.56 % for the fundamental frequency, 2.67 % for the second harmonic and 1.04 % for the third. No error estimation was done for the peak pressure due to the absence of a phase calibration of the hydrophone.

Highly focused beam

In order to test the algorithm in the very high nonlinear regime with realistic tissue parameters a focused bowl of geometrical focal $F = 50$ mm and aperture $A = 50$ mm, driven at $f_0 = 1$ MHz was numerically tested. These parameters leads to a source gain $G = 26.5$ and a f-number= 1, showing that source is beyond the paraxial limit. The media consist in two layers. The first, where the source was located, was water at 20^o with parameters $c_1 = 1482$ m/s, $\rho_1 = 1000$ kg/m^3, $B/A_1 = 5$, $\alpha_1 = 2.17 \times 10^{-3}$ dB/cm MHz$^\gamma$, $\gamma_1 = 2$. At a distance $z_l = 0.7/F = 35$ mm, a layer of human liver tissue was placed, therefore the focal spot is located inside tissue at a depth of 15 mm. Liver tissue parameters (Hill et al., 2004) were $c_2 = 1597$, $\rho_2 = 1050$ kg/m^3, $B/A_2 = 7.9$, $\alpha_2 = .75$ dB/cm MHz$^\gamma$, $\gamma_2 = 1.5$. In this case, the numerical grid parameters were $\Delta r = \Delta z = 29.6$ μm and $\Delta t = 11.9$ ns, leading to a CFL number $S = 0.9$ and $N_\lambda = 50$ elements per wavelength at fundamental frequency ($N_\lambda = 16$ for third harmonic).

Figure 7.16 shows the spatial peak pressure profiles for different excitation amplitudes. Thus, in Fig. 7.16 (top) the pressure of the source was $p_0 = 0.18$ MPa, while in the bottom figure was increased to $p_0 = 0.94$ MPa. Thus, for the selected parameters, Fig. 7.16 (top) present results for $\Gamma = 0.16$ and $N = 0.55$, so the attenuation effects dominates over nonlinear effects and nonlinearity dominates over diffraction effects. In this way, low asymmetry is observed between the positive compression peak, p^+, and the minimum rarefaction pressure distribution, p^-. The measured waveform at $z = F$, shown in the inset of Fig. 7.16 (top), is weakly distorted. However, there exist differences between its normalized peak amplitude $p^+/p_0 = 25.7$ and $p^-/p_0 = 21.05$, and the source characteristic linear gain, $G = 26.5$. There are caused, in one hand by the attenuation effects, where the value of the lossy linear gain observed was $G_\alpha = p^+/p_0 = p^-/p_0 = 23.1$ measured at z=F, i.e. the amplitude at the focal was reduced to 87.2% of the lossless amplitude. On the other hand, the differences due to the asymmetry between compression and rarefaction cycles are caused by the combined effect of nonlinearity and focusing.

If source amplitude is increased to $p_0 = 0.94$ MPa, as shown in Fig. 7.16 (bottom), the ratio between attenuation and nonlinear effects is increased to $\Gamma = 0.79$. In this regime, nonlinear effects are almost of the same order of attenuation effects. On the other hand, increasing source amplitude while keeping same transducer parameters implies also the Khoklov number changes to $N = 0.11$, so the nonlinear effects clearly dominates over diffraction. In this regime, highly asymmetric pressure distribution is observed, where the values at focal point are $p^+ = 49.05$ MPa and $p^- = -14.91$ MPa.

Other typical nonlinear phenomena characteristic of high intensity focused sources can also be observed: formation of sharp shock front and its corresponding harmonic generation, or, as Fig. (7.17) shows, narrowing of the beam for p^+ and broadening for p^- pressure distributions. In addition, nonlinear focal shift,

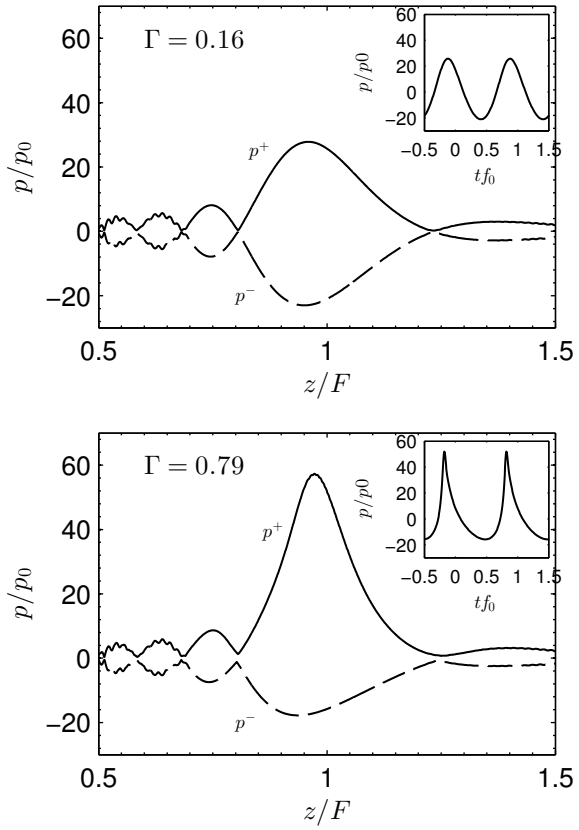


Figure 7.16: Axial spatial distribution of the peak compression (p^+) and minimum rarefaction (p^-) pressure for a focused transducer thought a liver tissue layer propagation. (Top) weakly nonlinear propagation ($\Gamma = 0.16$) and (bottom) strong nonlinear effects ($\Gamma = 0.79$). The insets show the waveforms recorded at the geometrical focal.

i.e. displacement of the peak pressure relative to the position of the liner peak pressure can be also predicted for tissue propagation. In the case of $\Gamma = 0.79$ the nonlinear focal shift was $\Delta F^+ = +1.05$ mm and $\Delta F^- = -1.03$ mm for the p^+ and p^- pressure distribution respectively.

7.6 Summary

A model for nonlinear acoustic waves in relaxing media is presented in a time-domain formulation which does not require convolutional operators. A numerical solution by means of finite-differences in time-domain have been obtained, showing that the theoretical attenuation and dispersion due to relaxation processes can be

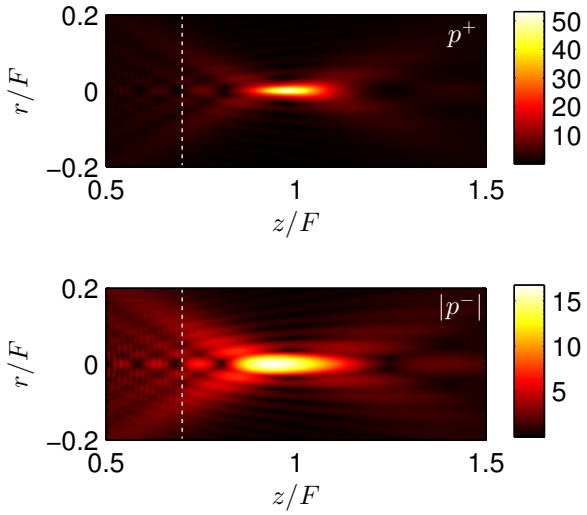


Figure 7.17: Spatial distribution of the peak compression (p^+) and minimum rarefaction (p^-) pressure for a focused transducer thought a liver tissue layer propagation (boundary marked with dashed line) for $\Gamma = 0.79$. Colorbars are in p/p_0 units.

achieved by the numerical method with accuracy. These result can be used to model typical relaxation process (e. g. the processes observed in air, associated to the molecules of oxygen and nitrogen, or in seawater, associated to the relaxation of boric acid and magnesium sulfate).

Moreover, a method for modeling a frequency power law on attenuation by means of multiple relaxation has been described. The proposed method can describe local variations of the exponent of the frequency power law, so an arbitrary attenuation curve in the range $0 < \gamma < 2$ can be modeled by means of the proper optimization of the relaxation coefficients. This feature of the presented method is an advantage when compared with most fractional derivatives methods, where the attenuation follows an exact but unique frequency power law over the entire frequency range. A broad range of human tissues have been modeled and the goodness of the fit using from two to four relaxation processes has been discussed.

Furthermore, a computational technique that exploits the *anomalous* dispersion of the relaxation processes is employed to mitigate the numerical dispersion of the finite-differences scheme. Thus, while phase speed is corrected by including artificial relaxation processes, its corresponding artificial attenuation is used to improve stability in the nonlinear regime. In this way, a smooth version of shock waves have been obtained and compared with analytic solutions. Furthermore, the validity of the algorithm including diffraction have been tested with experimental

measurements of a focused beam in castor oil.

Due to the model is developed from the constitutive relation for nonlinear acoustics, most wave phenomena is captured. As a difference from the one-way models the proposed model implicitly includes multiple wave direction, and, due to the Lagrangian density of acoustic energy is implicitly included in the computation, multiple scattering and strong resonance effects are accurately described. Moreover, unlike KZK and other parabolic approximations, the proposed model captures the diffraction exactly, so for simulation of acoustic beams the field is not approximated only to the beam axis, but also in the near field and far to the beam axis and thus high focusing devices can be simulated.

The code has shown to be particularly appropriate if the problem to simulate presents axisymmetry, because the constitutive relations for nonlinear acoustics are solved in a computational 2D domain, while standard k-space methods need to employ full 3D domains due to the poor convergence of the Fourier series at discontinuities ($r = 0$). This is the case, for example, of the focused transducer simulated in section 7.5.4, where a full 3D solution will require a huge computational resources and time. Finally, the particle velocity vector is solved implicitly by the code and can be used to estimate other relevant magnitudes as the full nonlinear intensity vector, the nonlinear radiation force field in the absorbing media or the acoustic streaming in frequency power law attenuation fluids.

References

Aanonsen, Sigurd Ivar, Tor Barkve, Jacqueline Naze Tjo, et al. (1984). "Distortion and harmonic generation in the nearfield of a finite amplitude sound beam". In: *J. Acoust. Soc. Am.* 75.3, pp. 749–768.

Albin, Nathan, Oscar P. Bruno, Theresa Y. Cheung, and Robin O. Cleveland (2012). "Fourier continuation methods for high-fidelity simulation of nonlinear acoustic beams". In: *J. Acoust. Soc. Am.* 132.4, pp. 2371–2387.

Blackstock, David T (1985). "Generalized Burgers equation for plane waves". In: *J. Acoust. Soc. Am.* 77.6, pp. 2050–2053.

Botteldooren, D. (1996). "Numerical model for moderately nonlinear sound propagation in three-dimensional structures". In: *J. Acoust. Soc. Am.* 100.3, pp. 1357–1367.

Canney, Michael S, Michael R Bailey, Lawrence A Crum, Vera A Khokhlova, and Oleg A Sapozhnikov (2008). "Acoustic characterization of high intensity focused ultrasound fields: A combined measurement and modeling approach". In: *The Journal of the Acoustical Society of America* 124.4, pp. 2406–2420.

Caputo, M. (1967). "Linear models of dissipation whose Q is almost frequency independent II". In: *Geophys. J. R. Astron. Soc.* 13, pp. 529–539.

Carstensen, EL, WK Law, ND McKay, and TG Muir (1980). "Demonstration of nonlinear acoustical effects at biomedical frequencies and intensities". In: *Ultrasound Med. Biol.* 6.4, pp. 359–368.

Chen, W and S Holm (2003). "Modified Szabos wave equation models for lossy media obeying frequency power law". In: *J. Acoust. Soc. Am.* 114.5, pp. 2570–2574.

Chen, W and S Holm (2004). "Fractional Laplacian time-space models for linear and nonlinear lossy media exhibiting arbitrary frequency power-law dependency". In: *J. Acoust. Soc. Am.* 115.4, pp. 1424–1430.

Christopher, P Ted and Kevin J Parker (1991). "New approaches to nonlinear diffractive field propagation". In: *J. Acoust. Soc. Am.* 90.1, pp. 488–499.

Cleveland, Robin O, Mark F Hamilton, and David T Blackstock (1996). "Time-domain modeling of finite-amplitude sound in relaxing fluids". In: *J. Acoust. Soc. Am.* 99.6, pp. 3312–3318.

Demi, L, KWA Van Dongen, and MD Verweij (2011). "A contrast source method for nonlinear acoustic wave fields in media with spatially inhomogeneous attenuation". In: *J. Acoust. Soc. Am.* 129.3, pp. 1221–1230.

Duck, Francis A. (1990). *Physical Properties of Tissue: A Comprehensive Reference Book.* San Diego, CA 92101, USA: Academic Press Inc. San Diego, p. 346.

Ginter, Siegfried, Marko Liebler, Eckard Steiger, Thomas Dreyer, and Rainer E. Riedlinger (2002). "Full-wave modeling of therapeutic ultrasound: nonlinear ultrasound propagation in ideal fluids." In: *J. Acoust. Soc. Am.* 111.5, pp. 2049–2059.

Goss, S. A., L. A. Frizzell, and F. Dunn (1979). "Ultrasonic absorption and attenuation in mammalian tissues". In: *Ultrasound Med. Biol.* 5 (2), pp. 181–186.

Hallaj, Ibrahim M and Robin O Cleveland (1999). "FDTD simulation of finite-amplitude pressure and temperature fields for biomedical ultrasound". In: *J. Acoust. Soc. Am.* 105.5, pp. L7–L12.

Hallaj, Ibrahim M, Robin O Cleveland, and Kullervo Hynynen (2001). "Simulations of the thermo-acoustic lens effect during focused ultrasound surgery". In: *The Journal of the Acoustical Society of America* 109.5, pp. 2245–2253.

Hamilton, M.F. and D.T. Blackstock (1998b). *Nonlinear Acoustics.* Academic Press.

Hill, C.R., J. C. Bamber, and G.R. ter Haar (2004). *Physical Principles of Medical Ultrasonics, 2nd ed.* John Wiley & Sons Ltd, Chichester, England.

Huijssen, Jacobus and Martin D Verweij (2010). "An iterative method for the computation of nonlinear, wide-angle, pulsed acoustic fields of medical diagnostic transducers". In: *J. Acoust. Soc. Am.* 127.1, pp. 33–44.

Jing, Yuan and Robin O Cleveland (2007). "Modeling the propagation of nonlinear three-dimensional acoustic beams in inhomogeneous media". In: *J. Acoust. Soc. Am.* 122.3, pp. 1352–1364.

Jing, Yun, Du Shen, and Greg T Clement (2011). "Verification of the Westervelt equation for focused transducers". In: *Ultrasonics, Ferroelectrics and Frequency Control, IEEE Transactions on* 58.5, pp. 1097–1101.

Jing, Yun, Tianren Wang, and Greg T Clement (2012). "A k-space method for moderately nonlinear wave propagation". In: *Ultrasonics, Ferroelectrics and Frequency Control, IEEE Transactions on* 59.8, pp. 1664–1673.

Jongen, HAH, JM Thijssen, M Van Den Aarssen, and WA Verhoef (1986). "A general model for the absorption of ultrasound by biological tissues and experimental verification". In: *The Journal of the Acoustical Society of America* 79.2, pp. 535–540.

Kellya, James F. and Robert J. McGough (2009). "Fractal ladder models and power law wave equations". In: *J. Acoust. Soc. Am.* 126.4, pp. 2072–2081.

Khokhlova, VA, AE Ponomarev, MA Averkiou, and LA Crum (2006). "Nonlinear pulsed ultrasound beams radiated by rectangular focused diagnostic transducers". In: *Acoustical Physics* 52.4, pp. 481–489.

Lee, Yang-Sub and Mark F Hamilton (1995). "Time-domain modeling of pulsed finite-amplitude sound beams". In: *J. Acoust. Soc. Am.* 97.2, pp. 906–917.

LeVeque, R.J. (1992). *Numerical Methods for Conservation Laws.* Ed. by Lectures in Mathematics. ETH Zurich. Birkhauser Verlag.

Liebler, Marko, Siegfried Ginter, Thomas Dreyer, and Rainer E. Riedlinger (2004). "Full wave modeling of therapeutic ultrasound: efficient time-domain implementation of the frequency power-law attenuation." In: *J. Acoust. Soc. Am.* 116.5, pp. 2742–2750.

Liu, Q. H. (1999). "Perfectly matched layers for elastic waves in cylindrical and spherical coordinates". In: *J. Acoust. Soc. Am.* 105.4, pp. 2075–2084.

Liu, Qing-Huo and Jianping Tao (1997). "The perfectly matched layer for acoustic waves in absorptive media". In: *J. Acoust. Soc. Am.* 102.4, pp. 2072–2082.

Lobanova, E. G., S. V. Lobanov, and V. A. Khokhlova (2014). "Counterpropagation of waves with shock fronts in a nonlinear tissue-like medium". In: *Acoustical Physics* 60.4, pp. 387–397.

Manry, Charles W and Shira L Broschat (1996). "FDTD simulations for ultrasound propagation in a 2-D breast model". In: *Ultrasonic imaging* 18.1, pp. 25–34.

Mast, T Douglas, Laura M Hinkelman, Michael J Orr, Victor W Sparrow, and Robert C Waag (1997). "Simulation of ultrasonic pulse propagation through the abdominal wall". In: *J. Acoust. Soc. Am.* 102.2, pp. 1177–1190.

Mast, T Douglas, Laurent P Souriau, D-LD Liu, Makoto Tabei, Adrian I Nachman, and Robert C Waag (2001). "A k-space method for large-scale models of wave propagation in tissue". In: *Ultrasonics, Ferroelectrics and Frequency Control, IEEE Transactions on* 48.2, pp. 341–354.

Muir, TG and EL Carstensen (1980). "Prediction of nonlinear acoustic effects at biomedical frequencies and intensities". In: *Ultrasound Med. Biol.* 6.4, pp. 345–357.

Nachman, Adrian I, James F Smith III, and Robert C Waag (1990). "An equation for acoustic propagation in inhomogeneous media with relaxation losses". In: *J. Acoust. Soc. Am.* 88, p. 1584.

Nasholm, Sven Peter and Sverre Holm (2011). "Linking multiple relaxation, power-law attenuation, and fractional wave equations". In: *J. Acoust. Soc. Am.* 130.5, pp. 3038–3045.

Naugolnykh, K. and L. Ostrovsky (1998). *Nonlinear Wave Processes in Acoustics*. Cambridge Texts in Applied Mathematics. Cambridge University Press.

Ochmann, Martin and Sergey Makarov (1993). "Representation of the absorption of nonlinear waves by fractional derivatives". In: *The Journal of the Acoustical Society of America* 94.6, pp. 3392–3399.

O'Donnell, M., E. T. Jaynes, and J. G. Miller (1981). "Kramers–Kronig relationship between ultrasonic attenuation and phase velocity". In: *J. Acoust. Soc. Am.* 69.3, pp. 696–701.

Pierce, A.D. (1989). *Acoustics: An Introduction to Its Physical Principles and Applications*. Acoustical Society of America.

Pinton, Gianmarco F, Jeremy Dahl, Stephen Rosenzweig, and Gregg E Trahey (2009). "A heterogeneous nonlinear attenuating full-wave model of ultrasound". In: *Ultrasonics, Ferroelectrics and Frequency Control, IEEE Transactions on* 56.3, pp. 474–488.

Prieur, Fabrice and Sverre Holm (2011). "Nonlinear acoustic wave equations with fractional loss operators". In: *J. Acoust. Soc. Am.* 130.3, pp. 1125–1132.

Rudenko, O.V. and S.I. Soluian (1977). *Theoretical foundations of nonlinear acoustics*. Studies in Soviet science. New York, NY 10011, USA: Consultants Bureau, p. 274.

Shahbazi, Khosro, Nathan Albin, Oscar P. Bruno, and Jan S. Hesthaven (2011). "Multi-domain Fourier-continuation/WENO hybrid solver for conservation laws". In: *J. Comput. Phys.* 230.24, pp. 8779 –8796.

Soneson, Joshua E and Matthew R Myers (2007). "Gaussian representation of high-intensity focused ultrasound beams". In: *The Journal of the Acoustical Society of America* 122.5, pp. 2526–2531.

Sparrow, Victor W and Richard Raspet (1991). "A numerical method for general finite amplitude wave propagation in two dimensions and its application to spark pulses". In: *J. Acoust. Soc. Am.* 90.5, pp. 2683–2691.

Szabo, Thomas L (1994). "Time domain wave equations for lossy media obeying a frequency power law". In: *J. Acoust. Soc. Am.* 96.1, pp. 491–500.

Tavakkoli, Jahangir, Dominique Cathignol, Rémi Souchon, and Oleg A Sapozhnikov (1998). "Modeling of pulsed finite-amplitude focused sound beams in time domain". In: *The Journal of the Acoustical Society of America* 104.4, pp. 2061–2072.

Treeby, Bradley E, Benjamin T Cox, Edward Z Zhang, Sarah K Patch, and Paul C Beard (2009). "Measurement of broadband temperature-dependent ultrasonic attenuation and dispersion using photoacoustics". In: *Ultrasonics, Ferroelectrics, and Frequency Control, IEEE Transactions on* 56.8, pp. 1666–1676.

Treeby, Bradley E and BT Cox (2010). "Modeling power law absorption and dispersion for acoustic propagation using the fractional Laplacian". In: *J. Acoust. Soc. Am.* 127.5, pp. 2741–2748.

Treeby, Bradley E, Jiri Jaros, Alistair P Rendell, and BT Cox (2012). "Modeling nonlinear ultrasound propagation in heterogeneous media with power law absorption using a k-space pseudospectral method". In: *J. Acoust. Soc. Am.* 131.6, pp. 4324–4336.

Varslot, Trond and Gunnar Taraldsen (2005). "Computer simulation of forward wave propagation in soft tissue". In: *Ultrasonics, Ferroelectrics and Frequency Control, IEEE Transactions on* 52.9, pp. 1473–1482.

Verweij, Martin D, Libertario Demi, and Koen WA van Dongen (2013). "Computation of nonlinear ultrasound fields using a linearized contrast source method". In: *J. Acoust. Soc. Am.* 134.2, pp. 1442–1453.

Waters, Kendall R, Joel Mobley, and James G Miller (2005). "Causality-imposed (Kramers-Kronig) relationships between attenuation and dispersion". In: *Ultrasonics, Ferroelectrics and Frequency Control, IEEE Transactions on* 52.5, pp. 822–823.

Wismer, M. G. (2006). "Finite element analysis of broadband acoustic pulses through inhomogeneous media with power law attenuation". In: *J. Acoust. Soc. Am.* 120, pp. 3493–3502.

Wismer, Margaret G and Reinhold Ludwig (1995). "An explicit numerical time domain formulation to simulate pulsed pressure waves in viscous fluids exhibiting arbitrary frequency power law attenuation". In: *Ultrasonics, Ferroelectrics and Frequency Control, IEEE Transactions on* 42.6, pp. 1040–1049.

Yang, Xinmai and Robin O Cleveland (2005). "Time domain simulation of nonlinear acoustic beams generated by rectangular pistons with application to harmonic imaging". In: *J. Acoust. Soc. Am.* 117.1, pp. 113–123.

Yuan, Xiaojuen, D. Borup, J. Wiskin, M. Berggren, and S. A. Johnson (1999). "Simulation of acoustic wave propagation in dispersive media with relaxation losses by using FDTD method with PML absorbing boundary condition". In: *IEEE Transactions on Ultrasonics, Ferroelectrics, and Frequency Control* 46.1, pp. 14–23.

Yuldashev, PV and VA Khokhlova (2011). "Simulation of three-dimensional nonlinear fields of ultrasound therapeutic arrays". In: *Acoustical physics* 57.3, pp. 334–343.

Zemp, Roger J, Jahangir Tavakkoli, and Richard SC Cobbold (2003). "Modeling of nonlinear ultrasound propagation in tissue from array transducers". In: *J. Acoust. Soc. Am.* 113.1, pp. 139–152.

Publications

The contents of this chapter have been presented in the following publications:

Journal papers

- **Jiménez, N.**; Camarena, F.; Redondo, J.; Sánchez-Morcillo, V.; Hou Y. and Konofagou E. E. "Time-domain simulation of ultrasound propagation in tissue-like medium based on the resolution of the nonlinear acoustic constitutive relations". *The Journal of Acoustical Society of America*, *In preparation.*

Conference proceedings

- **Jiménez, N.**, F. Camarena, V. Sanchez-Morcillo, J. Redondo and E.E. Konofagou. "Time-domain simulation of constitutive relations for nonlinear acoustics including relaxation for frequency power law attenuation media modelling". *ISNA 2015,*

International Symposium of Nonlinear Acoustics. June 29th - July 3rd 2015, Lyon, France (2015).

- **Jiménez, N.**; Redondo, J.; Sánchez-Morcillo, V. and Camarena, F. "Nonlinear ultrasound simulations including complex frequency dependent attenuation". *43rd Annual UIA Symposium*, Madrid, Spain. 23 - 25 April. *Physics Procedia*, Volume 63, 2015, Pages 108-113, (2014)
- **Jiménez, N.**; Redondo, J.; Sanchez-Morcillo, V. and Camarena, F. "Ondas acústicas de amplitud finita en medios con relajación: aplicación a la modelización de tejidos biológicos". *44º Tecniacústica'13*, Valladolid, October, 1632-1637 (2013)

And the numerical method method have been applied for obtaining the following results

Journal papers

- **Jiménez, N.**; Redondo, J.; Sanchez-Morcillo, V. and Camarena, F. "Numerical Study of Nonlinear, Transcranial Focused Ultrasound Wave Propagation for Blood-Brain Barrier Opening". *IEEE Ultrasonics, Ferroelectrics and Frequency Control Society*, *In preparation.*
- **Jiménez, N.**; Marquet, F.; Camarena, F.; Konofagou, E. E.; Redondo, J.; Roig, B. and Picó, R. "Estudio de la propagación no lineal de haces de ultrasonidos focalizados a través del cráneo para la apertura de la barrera hematoencefálica". *Revista de Acústica*, 43, 5-11 (2012)

Conference proceedings

- Ordoñez-Cebrián, P; **Jiménez, N.**; Espinosa, V.; Puig-Pons, V. and Soliveres-González, E. "Efficiency of parametric ultrasound generation in relaxing media for very shallow-water echo sounders". *43rd Annual UIA Symposium.* Madrid, Spain. 23-25 April, (2014)
- Iglesias, P. C.; **Jiménez, N.**; Konofagou, E.; Camarena, F. and Redondo, J. "Transcranial Propagation with an Ultrasonic Mono-Element Focused Transducer". *43rd Annual UIA Symposium*, Madrid, Spain. 23-25 April. *Physics Procedia* Volume 63, 2015, Pages 103-107, (2014)
- Iglesias, P. C.; **Jimenez, N.**; Redondo, J.; Konofagou, E. E. and Camarena, F. "Parametric study of transcranial focused ultrasound propagation for blood–brain barrier opening". *European Symposium on Ultrasonic Characterization of Bone*. Granada, 7-10 May, (2013)
- **Jiménez, N.**; Roig, B.; Redondo, J.; Pico, R.; Marquet, F.; Konofagou, E. E. and Camarena, F. "Numerical study of nonlinear, transcranial focused ultrasound wave propagation for blood-brain barrier (BBB) opening". *ISTU 2011: International Society for Therapeutic Ultrasound Symposium*, New York, EEUU, (2011)